2020 IEEE International Conference on Robotics and Automation (ICRA)
31 May - 31 August, 2020. Paris, France

Pressure-Driven Manipulator with Variable Stiffness Structure

Canberk Sozer, Linda Paternò, Giuseppe Tortora, Arianna Menciassi

Abstract— **The high deformability and compliance of soft robots allow safer interaction with the environment. On the other hand, these advantages bring along controllability and predictability challenges which result in loss of force and stiffness output. Such challenges should be addressed in order to improve the overall functional performance and to meet the requirements of real-scenario applications. In this paper, we present a bidirectional in-plane manipulator which consists of two unidirectional fiber-reinforced actuators (FRAs) and a hybrid soft-rigid stiffness control structure (SCS), all of them controlled by air pressure. Both controllability and predictability of the manipulator are enhanced by the hybrid soft-rigid structure. While the FRAs provide positioning and position dependent stiffness, the SCS increases the stiffness of the manipulator without position dependency. The SCS is able to increase the manipulator stiffness by 35%, 30%, and 18%, when one FRA is pressurized at 150 kPa, 75 kPa, and 0 kPa, respectively. Experiments are carried out to present the feasibility of the proposed manipulator.**

I. Introduction

In robotic manipulators, the ability to change the joint stiffness allows to choose if resisting or complying with external forces during the interaction with the environment [1, 2]. In traditional robotic manipulators, actuators are selected to be as stiff as possible to accomplish more precise position movements and trajectory tracking control. However, the increment of human-centered robotic applications has made necessary a drastic change of the main requirements, focusing the attention on safety. In the last decades, soft robotics has attempted to offer a feasible solution for safe physical human-robot interactions [3]. Nevertheless, soft manipulators are generally able to produce lower output forces and less precise movements. For this reason, the design of actuators able to tune their stiffness could represent an efficient solution for combining the advantages of both rigid and soft systems, thus overcoming some of their limitations.

In this framework, various variable stiffness methods were applied widely to soft robots, e.g. pneumatic based [4-6], jamming based [7-9], shape memory polymers based [10-12], low melting point alloy based [13-15].

Recently the hybridization concept of rigid and soft materials has been explored [16]. The final aim is to preserve the compliance and safety of completely soft manipulators by adopting a solution for addressing controllability and large force delivery issues. In the current state of the art, some recent examples are presented, reporting tunable stiffness methods based on active [17, 18] and passive [19, 20] solutions, thus confirming the increasing interests of researchers towards hybrid soft-rigid approach. An interesting example of the hybrid soft-rigid manipulator is proposed by Su *et al.* [21]. This manipulator consists of a pneumatic soft actuator with anisotropic soft and rigid restraints in the central part. The central hybrid structure is characterized by a metal hinge belt embedded into the soft material. This allows a pure in-plane bending motion with different stiffness values in different manipulator configurations. The main drawback is the inability to tune a specific stiffness value in all the possible configurations, thus limiting the manipulator controllability.

This work presents a new manipulator which is composed of two fiber-reinforced soft actuators (FRAs) interfaced with a hybrid soft-rigid stiffness control structure (SCS) in the central part. The main motivation of the proposed structure is to tune the manipulator stiffness by simple air pressure, without position dependency and interference. The final position can be bidirectionally controlled in-plane by the pneumatic manipulator when the SCS is not actuated. Moreove[1]r, the reached configuration can be become stiff by pressurizing the SCS joints, allowing the manipulator to provide position-independent variable stiffness. As a result, the hybrid soft-rigid approach enables to develop a variable stiffness manipulator which is repeatable, but also low cost.

The manipulator can be used for different applications in health, industry and other specific scenarios in which soft actuators are required for improving the safety, but also an adequate stiffness and dexterity are essential features to be achieved.

II. Design of the Manipulator

The designed manipulator is shown in Fig. 1. The bidirectional manipulator consists of an SCS inside an encapsulation layer and two identical FRAs both placed on each side of the layer. While the FRAs control the position of the manipulator, the SCS provides the variable stiffness. The FRAs and the SCS are driven by air pressure aiming to minimize the control complexity and response time while providing position independent stiffness.

A. Fiber-Reinforced Actuator

The FRA (Fig. 2) is designed in semi-circular geometry to minimize the resistance to bending of the pressurized actuator [22]. The FRA is the manipulator module for providing the bending to the entire structure. The body of the FRA is made of DragonSkin 10 (Shore Hardness: 10A, Smooth-On Inc., USA) silicone rubber, whereas DragonSkin 30 (Shore Hardness: 30A, Smooth-On Inc., USA) rubber was used for capping due to its higher hardness. Each FRA

* This work was supported in part by the Scuola Superiore Sant'Anna and in part by the MOTU (robotic prosthesis with sMart sOcket and bidirectional inTerface for lower limb ampUtees) project which is funded by INAIL (Istituto Nazionale Assicurazione Infortuni sul Lavoro).

All the authors are with The BioRobotics Institute and Department of Excellence in Robotics & AI, Scuola Superiore Sant'Anna Pisa, Viale Rinaldo Piaggio 34 Pontedera, PI 56025 Italy. Canberk Sozer is the corresponding author with e-mail: canberk.sozer@santannapisa.it.

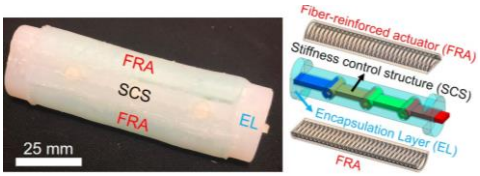

Figure 1. Prototype (left) and solid model (right) of the developed manipulator. FRA: Fiber-reinforced actuator, SCS: Stiffness control structure and EL: Encapsulation layer.

is controlled by one input pressure and is able to bend unidirectionally. Thus, two identical FRAs are used to achieve bidirectional bending.

Since entirely soft actuators may face controllability and predictability issues when pressurized, the presented silicone-based FRAs are mechanically constrained [23, 24] to obtain desired actuation performance. An inextensible nylon fiber as a fiber-reinforcement element is used to overcome these issues. The fiber is wound along the length of the FRA in double-helix configuration (*i.e.* clockwise and counterclockwise). It is embedded in the middle of the bilayer actuator to minimize lateral expansion while supporting the extension of the pressurized FRA.

Upon pressurizing, the extension of the FRA is constrained by the encapsulation layer which is made of stiffer material as a strain limiting element. Meanwhile, the extension causes curvature because of the stiffness difference [25] between the materials of the FRA (Shore Hardness: 10A) and the encapsulation layer (Shore Hardness: 30A). In addition to its strain limiting purpose, it integrates the SCS with the FRAs.

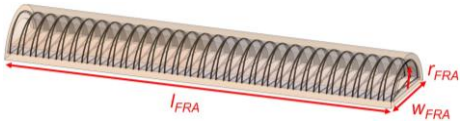

Figure 2. View of the FRA with wrapped fiber element (black helix). l_{FRA}: 90 mm, w_{FRA}: 20 mm, r_{FRA}: 7 mm.

B. *Stiffness Control Structure*

The proposed stiffness concept is composed of modular rigid links and soft pressure chambers which are made of UV curable plastic and DragonSkin 10, respectively. By the integration of two rigid links using alignment pins, a rigid compartment in a revolute joint form appears, then a pressure chamber is positioned in it (Fig. 3a). Lateral and axial expansions of the pressurized chamber are constrained by the rigid compartment. Upon pressurization, the stress at the contact surface between the pressure chamber and the rigid compartment increases. This causes increasing friction at the surface and resultant stiffness of the joint (Fig. 3b). As a result, the stiffness can be easily controlled by the input pressure.

The SCS includes three joints (*i.e.* four rigid links and three pressure chambers), all of them controlled independently (Fig. 3c). The entire SCS was aimed to be rotated between -90° - +90° in the x-y plane, thus the rotation of each joint is mechanically limited between -30° - +30° around their axial direction to add up 90°. Thanks to the modular design of the rigid links, the total rotation angle can be increased or decreased by changing the number of rigid links.

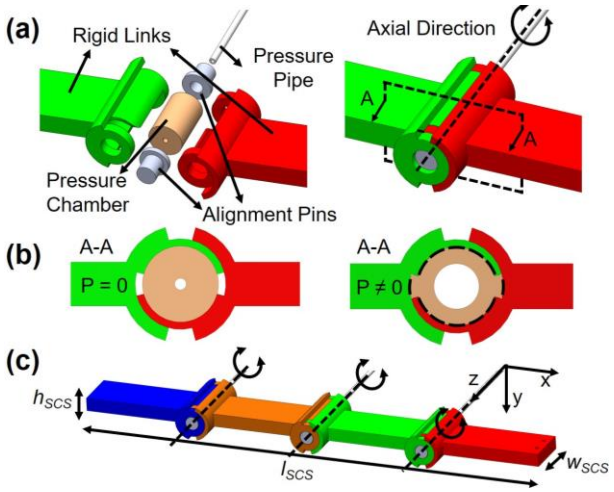

Figure 3. (a) Components of the hybrid soft-rigid joint concept (left), assembled joint (right), (b) A-A cross section of assembled joint with unpressurized (left) and pressurized (right) pressure chambers in the rigid compartment (by pressurization, increasing stress at the contact surface is represented by dashed black line), (c) assembled SCS. l_{SCS}: 100 mm, w_{SCS}: 10 mm, h_{SCS}: 8 mm.

III. Fabrication Process

All the rigid parts of the SCS and molds for silicone casting were designed using SolidWorks (Dassault Systèmes, France) and fabricated by ProJet 3600 HD Max (3D Systems, USA) 3D printer using UV curable plastic (VisiJet M3 Crystal, 3D Systems, USA). The fabrication consists of four steps: *i)* fabrication of the FRAs; *ii)* preparation of the SCS and its encapsulation layer; *iii)* integration; *iv)* capping. After fabrication, the manipulator is properly assembled as shown in Fig. 4.

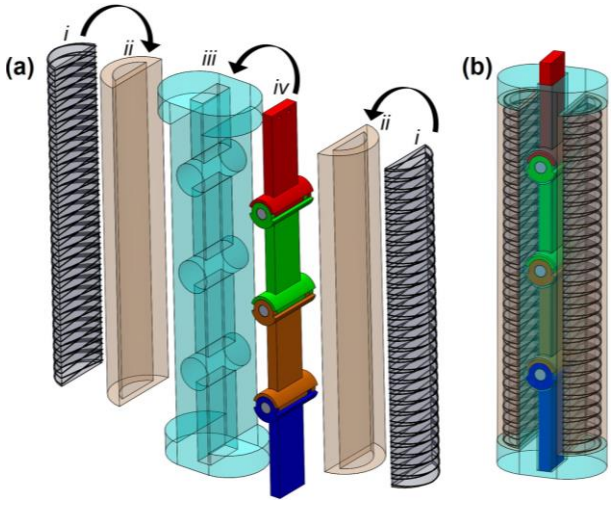

Figure 4. (a) Components of the manipulator: *i)* inextensible nylon fiber as a reinforcement element, ii) unreinforced silicone actuator, *iii)* encapsulation layer, *iv)* SCS. (b) completed manipulator.

A. *FRA fabrication*

Each FRA is fabricated in 3 steps: *i)* first silicone layer fabrication; *ii)* fiber winding; *iii)* second silicone layer fabrication. The A and B parts of the DragonSkin 10 were mixed equally by weight and degassed to eliminate entrapped air bubbles. The mixture was poured into the first mold (Fig. 5a) for the first layer of the FRA. When the silicone is cured

completely, 0.3 mm inextensible nylon fiber was wound with 1.5 mm pitch (Fig. 5b). Then, it was placed in the second mold and the second layer of the DragonSkin 10 was poured (Fig. 5c). The process was repeated one more time to fabricate the second FRA (Fig. 5d).

B. SCS fabrication

To fabricate pressure chambers for the SCS, the prepared DragonSkin 10 was poured into the pressure chamber molds and a straight mold was placed at the middle for the inflation channel (Fig. 5e). Two alignment pins and a pressure pipe were glued to the cured chamber by silicone glue (Fig. 5f). These processes were repeated two more times to fabricate three identical pressure chambers for joints. The completed chambers were placed into the appearing rigid compartments by the integration of the rigid links (Fig. 5g).

To fabricate the encapsulation layer, the prepared DragonSkin 30 was poured into the encapsulation layer molds and a second mold part was placed in the center to leave a space for the SCS (Fig. 5h). After the layer is cured (Fig. 5i), the SCS is placed into the dedicated opening.

The separately fabricated FRAs (Fig. 5d), the SCS (Fig. 5g), and the encapsulation layer (Fig. 5i) were assembled (Fig. 5j).

As the final step, the prepared DragonSkin 30 was poured into a capping mold, then both sides of the assembled manipulator were dipped into the mold one by one. The pressure pipes for the FRA actuation were inserted and fixed by silicone glue (Fig. 5k-l).

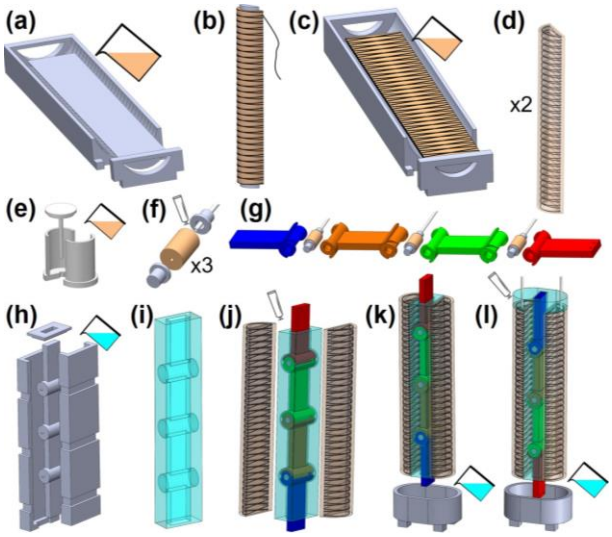

Figure 5. (a) Pouring DragonSkin 10 silicone into the mold of the first layer of the FRA, (b) fiber wrapping, (c) pouring DragonSkin 10 into the mold of the second layer of the FRA, (d) completed FRA, (e) pouring DragonSkin 10 into pressure chamber mold, (f) integration of the cured pressure chamber with the alignment pins and a pressure pipe, (g) assembly of the SCS parts, (h) pouring DragonSkin 30 silicone into the mold of encapsulation layer, (i) completed encapsulation layer, (j) gluing FRAs, the SCS and the encapsulation layer, (k-l) capping and pressure pipe integration.

IV. RESULTS

The manipulator was characterized in terms of compliance, stiffness capability and workspace. All tests were performed in the x-y plane, with reference to Fig. 6, by compensating the gravity. For clarification, the pressurized

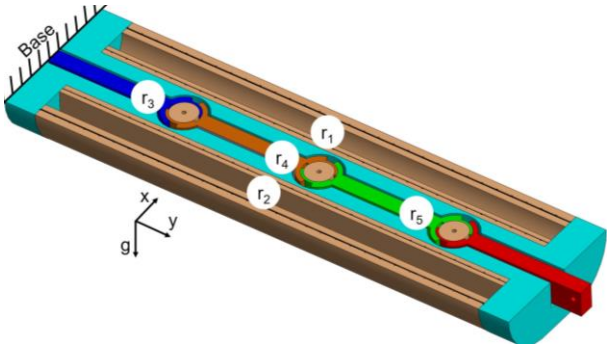

Figure 6. r_1 and r_2 represent FRAs. r_3, r_4, and r_5 represent the pressure chambers from the base to the end effector. g: gravity force.

regions are named as r_i (i = 1, 2, 3, 4, 5). While the r_1 and r_2 represent the FRAs, the r_3, r_4 and r_5 represent the joints of the SCS from proximal to distal part. To actuate the manipulator, only one (r_1) of the two FRAs is pressurized at a time. On the other hand, the joints of the SCS are pressurized together with the same pressure to demonstrate the maximum stiffness contribution of the SCS to the manipulator.

For the compliance, SCS stiffness and controllable stiffness tests, force data were collected. Then, the stiffness was evaluated from the collected force data by using $k = Fx/r$ where k is rotational stiffness, F is force data, x is displacement and r is rotation angle in radian. To clarify the evaluation scheme, the displacement and the mean with the standard deviation of the 10 measured angles are given in Table I to be used in the following experiments.

TABLE I. THE APPLIED DISPLACEMENTS AND RESULTANT ROTATION ANGLES OF THE TESTED CONDITIONS.

Test Name	x [mm]	Angle [°]
Compliance Test		
0 kPa	30	16.4 ± 0.13
30 kPa		16.1 ± 0.03
60 kPa		14 ± 0.08
90 kPa		13.7 ± 0.04
120 kPa		13.9 ± 0.14
150 kPa		14 ± 0.12
SCS Stiffness Test		
1 Joint	5	2.9 ± 0.11
2 Joints	15	7.8 ± 0.46
3 Joints	30	13.1 ± 0.28
Controllable Stiffness Test		
0 kPa	30	16.4 ± 0.13
75 kPa		14.7 ± 0.05
150 kPa		14 ± 0.12

A. Compliance Test

A Nano 17 (ATI Industrial Automation, USA) force sensor which was attached to an RV-3SB (Mitsubishi Industrial Robot, Japan) robot arm was used to investigate how the SCS affects the compliance of the manipulator. During the experiments, the manipulator, with and without the SCS, was fixed in a lateral configuration to avoid gravity effect in the results. Then, the inlet pressure of r_1 was increased from 0 kPa to 150 kPa at a step of 30 kPa while the joints of the SCS are not pressurized. At each step, the manipulator end effector was pulled 30 mm along the x-axis at 5 mm/s speed by the robot arm. The mean and the standard

deviation of 10 trials are reported in Fig. 7. Results show that the manipulator stiffness has partial nonlinearities with the increasing pressure depending on the bending angle of the manipulator in both situations (*i.e.* with and without the SCS). Also, it was calculated that the SCS increases (decreases) the manipulator stiffness (compliance) by 30% on average.

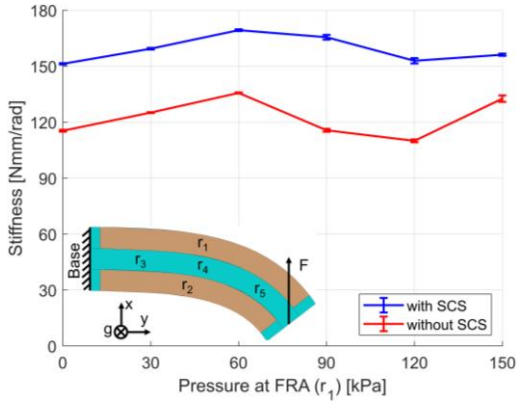

Figure 7. Experimental result of the input pressure to r_1 - manipulator stiffness relationship with and without SCS. The mean and the standard deviation of the 10 trials are given.

B. SCS Stiffness Test

The stiffness capability of the SCS was assessed by characterizing one joint (r_3), two joints (r_3 and r_4) and the completed SCS (r_3, r_4, and r_5). Tests were carried out by pressurizing the internal pressure chambers from 0 kPa to 600 kPa at 100 kPa step. Since the SCS has a rigid compartment surrounding the pressure chamber, it was tested under higher pressure comparing to the FRA (150 kPa) which is made of softer material. The Nano 17 force sensor was attached to the robot arm to pull the distal end 30 mm (in three joints case), 15 mm (in two joints case) and 5 mm (in one joint case) along the x-axis at 5 mm/s speed. In Fig. 8, the mean and the standard deviation of 10 trials for the three configurations are shown. Results show that increasing the inlet pressure provides an increment of the joint stiffness which ranges from 10 to 58 Nmm/rad (increased by 480%) for three joints, 17 to 70 Nmm/rad (increased by 312%) for two joints and 15 to 108 Nmm/rad (increased by 620%) for one joint.

C. Position Tests

In order to assess the end effector paths of the manipulator with and without SCS configurations, the FRA (r_1) was pressurized and depressurized. The end effector was tracked by the Aurora (Northern Digital, Canada) magnetic tracking system (Fig. 9). The position tests were conducted in 3 steps: *i)* the manipulator was fixed at its initial position (0°); *ii)* r_1 was pressurized from 0 kPa to 150 kPa at a step of 30 kPa; *iii)* r_1 was depressurized from 150 kPa to 0 kPa at a step of 30 kPa to back to the initial position. During the position test, r_2 is not pressurized. The sequence was repeated 10 times for both configurations (*i.e.* with and without the SCS). The mean of the end effector positions in the x-y plane and the calculated angles are given with their standard deviations in Table II.

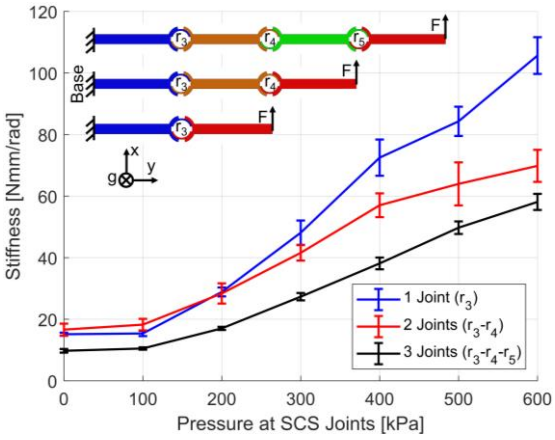

Figure 8. Experimental results of the input pressure (at r_3, r_3 - r_4 and r_3 - r_4 - r_5) - joint stiffness relationship. The mean and the standard deviation of the 10 trials are given.

The mean of the maximum bending angle of the manipulator was calculated as 37° (without the SCS) and 24.7° (with the SCS) at 150 kPa. The rigid construction of the SCS limited the bending angle as expected. On the other hand, the SCS causes the changing of the path which followed by the end effector. As shown in Table II, all the standard deviations are equal or lower in the case of the manipulator with the SCS compared to the manipulator without the SCS. So, it can be said that the presence of the SCS decreases the variation of the position at a specific pressure value and increases the precision of the manipulator consequently. In case of the manipulator without the SCS, the maximum standard deviations of the end effector are 0.53 mm along the x-axis, 0.69 mm along the y-axis and 0.46° for bending angle during pressurization and depressurization. On the other hand, the maximum standard deviations are 0.44 mm along the x-axis, 0.25 mm along the y-axis and 0.29° for bending angle in case of the manipulator with the SCS. Thus, the existence of the SCS improves the precision of the end effector positioning by 20% along the x-axis, 176% in the y-axis and 59% in bending.

In addition, when the FRA is depressurized, the manipulator returns to 0.2° (manipulator with the SCS) and 0.3° (manipulator without the SCS) due to the elastic energy stored in the silicone parts (*i.e.* FRAs, encapsulation layer, and pressure chambers of the SCS joints) of the manipulator.

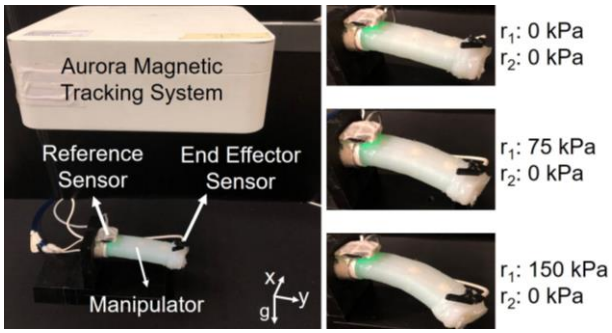

Figure 9. Experimental setup for magnetic position tracking. The prototype lays on an horizontal table.

TABLE II. POSITION OF THE MANIPULATOR END EFFECTOR WITH AND WITHOUT THE SCS DURING PRESSURIZATION AND DEPRESSURIZATION. THE RESULTS ARE GIVEN IN THE X-Y PLANE. RED AND BLUE TONES REPRESENT THE MANIPULATOR WITHOUT AND WITH THE SCS, RESPECTIVELY.

		Manipulator without SCS			Manipulator with SCS		
		x [mm]	y [mm]	Angle [°]	x [mm]	y [mm]	Angle [°]
Pressurization	0 kPa	0	102	0	0	102	0
	30 kPa	7.7 ± 0.27	103 ± 0.05	3.8 ± 0.14	5.4 ± 0.13	102 ± 0.05	2.5 ± 0.07
	60 kPa	19 ± 0.38	102.4 ± 0.08	10 ± 0.2	13.5 ± 0.22	101.7 ± 0.05	7.1 ± 0.12
	90 kPa	35 ± 0.53	98.3 ± 0.23	19.1 ± 0.3	24.2 ± 0.34	99.7 ± 0.11	13.2 ± 0.19
	120 kPa	52.7 ± 0.45	88.3 ± 0.43	30.4 ± 0.32	36.3 ± 0.29	95.5 ± 0.14	20.4 ± 0.18
	150 kPa	61.3 ± 0.48	80.1 ± 0.69	37 ± 0.46	43.2 ± 0.44	92 ± 0.25	24.7 ± 0.29
Depressurization	120 kPa	55.4 ± 0.24	86.1 ± 0.26	32.3 ±0.17	40.3 ± 0.14	93.5 ± 0.08	22.9 ± 0.11
	90 kPa	40.2 ± 0.37	95.9 ± 0.26	22.3 ± 0.23	30.8 ± 0.22	98.1 ± 0.07	17 ± 0.14
	60 kPa	23.4 ± 0.4	101.5 ± 0.13	12.5 ± 0.22	19.2 ± 0.23	101.2 ± 0.05	10.3 ± 0.13
	30 kPa	10.6 ± 0.29	103 ± 0.1	5.4 ± 0.15	9.3 ± 0.16	102.2 ± 0.02	4.8 ± 0.08
	0 kPa	1.4 ± 0.13	102 ± 0.06	0.3 ± 0.07	1.4 ± 0.1	102 ± 0.03	0.2 ± 0.04

D. *Controllable Stiffness Test*

The FRAs (*i.e.* r_1 and r_2) are the same for symmetry, thus the FRA (r_1) and joints of the SCS (*i.e.* r_3, r_4, and r_5) were pressurized in various combinations to investigate the controllable stiffness of the manipulator. The SCS joints were pressurized up to 600 kPa with 100 kPa step to provide the stiffness. Tests were carried out while the FRA was: *i)* not pressurized; *ii)* pressurized at 75 kPa; *iii)* pressurized at 150 kPa.

The end effector of the manipulator was pulled 30 mm along the x-axis at 5 mm/s speed by the Nano 17 force sensor attached to the robot arm through an inextensible fiber as shown in Fig. 10. All the tests were repeated 10 times to improve statistical significance.

The results are given in Fig. 11. As expected, the SCS allows controlling the stiffness of the manipulator by increasing the pressure. The SCS increases the manipulator stiffness from 156 to 211 Nmm/rad (increased by 35%), from 156 to 203 Nmm/rad (increased by 30%) and from 151 to 178 Nmm/rad (increased by 18%), if the FRA (r_1) is pressurized at 150 kPa, 75 kPa and 0 kPa, respectively.

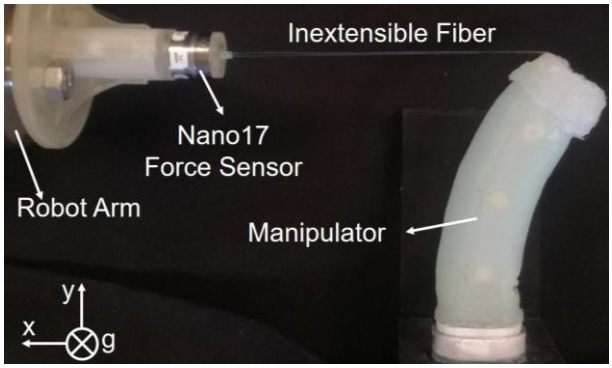

Figure 10. Experimental setup for manipulator stiffness measurement.

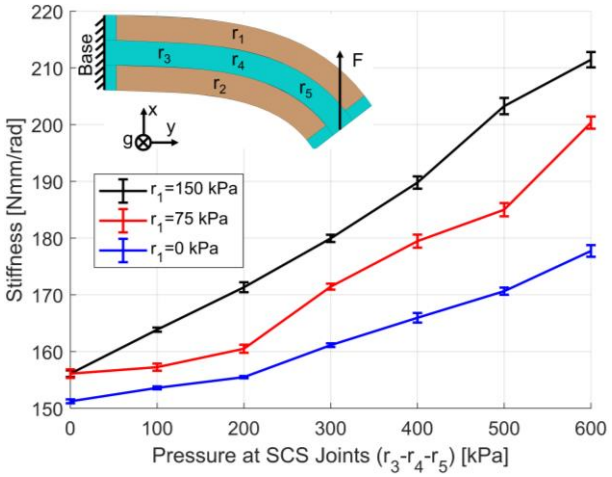

Figure 11. Experimental results of the input pressure - manipulator stiffness relationship. The mean and the standard deviation of the 10 trials are given.

V. DISCUSSION AND CONCLUSION

In this study, we presented a variable stiffness manipulator to address the predictability and controllability challenges of soft robotics. The manipulator consists of two fiber-reinforced actuators (FRAs) and hybrid soft-rigid stiffness control structure (SCS), all of them controlled by simple air pressure. The FRAs are mainly used for positioning, but their stiffness depends on its position. Meanwhile, the SCS is used to tune the stiffness of the manipulator without position dependency.

Each FRA has unidirectional motion capacity. On the other hand, the SCS was designed in a revolute joint form, thus its bidirectional motion ability is limited in-plane. A manipulator was assembled by intersecting the bending planes of the FRAs and SCS, which is able to move bidirectionally in-plane. Therefore, all the compliance, position, and stiffness capability tests were conducted in the x-y plane.

The compliance test shows that increasing pressure causes partial nonlinearities in measured stiffness. To be

noted that, adding the SCS into the manipulator reduces the compliance of the manipulator by 30% on average. It is a cost of increasing the manipulator precision and providing controllable stiffness.

The SCS stiffness test was conducted to characterize the maximum stiffness contribution of the SCS. In order to do that three different configurations (*i.e.* one having one joint, one having two joints and one having three joints) were tested by pressurizing their joints at 600 kPa. As a result, the stiffness increased by 620%, 312%, and 480% for configurations with one joint, two joints and three joints, respectively. It could be interesting to investigate what happens if the joints are pressurized at different values with various pressurization sequence. In that case, they do not only provide partial stiffness on the same body without any modification on the base structure but also allow to form the manipulator in S-like patterns.

The position test was conducted to define the end effector path in two ways: the manipulator with the SCS and the manipulator without the SCS. For each case, 10 trials were done to investigate the path during pressurization at 150 kPa and depressurization. After depressurization, the manipulator returns to 0.3° (manipulator without the SCS) and 0.2° (manipulator with the SCS) which is acceptable in terms of hysteresis. If a better performance (*i.e.* less than 0.2°) is expected, an extra energy storage element (*i.e.* spring) can be integrated into the manipulator, but it reduces the overall compliance.

Adding the SCS into the manipulator changes the followed path of the end effector. The manipulator reaches the maximum angle of 37° (the manipulator without the SCS) and 24.7° (the manipulator with the SCS) through following different paths. Thus, end effector precision to follow their own paths was evaluated by comparing the standard deviation of the 10 trials for both configurations. Results show that adding the SCS into the manipulator increases the precision of the manipulator by 20% along the x-axis, by 176% along the y-axis and by 59% for bending. We believe this is a promising improvement to address the precision challenge of soft robotics. Modeling of the manipulator is out of the scope for this study. In future, it could be interesting to evaluate the accuracy of the end effector by comparing an analytical model with experimental results.

When all the joints of the SCS are pressurized from 0 to 600 kPa, the manipulator stiffness increases from 156 to 211 Nmm/rad, from 156 to 203 Nmm/rad and from 151 to 178 Nmm/rad if pressure at the FRA is 150 kPa, 75 kPa, and 0 kPa, respectively. By increasing the pressure at the SCS joints, the stiffness of the manipulator increases linearly. These results show that the proposed hybrid soft-rigid concept is a good candidate to tune the stiffness by simple air pressure.

Future works include miniaturization of the proposed prototype, sensorization of the system, but also providing motion ability in 3D space by using spherical joints in SCS while keeping its modularity. In particular, we will focus on implementing the proprioception sensing strategy by integrating deformable and stretchable sensors inside the actuators while keeping the hybrid soft-rigid concept. The sensor data obtained from the embedded sensors in the actuator will be used as feedback for the closed-loop control, which will be developed. This approach will allow fixing the manipulator at a desired position against the disturbances in an unknown environment.

REFERENCES

[1] R Ham, T Sugar, B Vanderborght, K Hollander, and D Lefeber. Compliant actuator designs. *IEEE Robot. Autom. Mag.*, vol. 16, no. 3, pp. 81–94, Sep. 2009.

[2] A Pervez and J Ryu. Safe physical human robot interaction-past, present and future. *J. Mech. Sci. Technol.*, vol. 22, no. 3, pp. 469–483, Mar. 2008.

[3] M Manti, V Cacucciolo, and M Cianchetti. Stiffening in Soft Robotics: A Review of the State of the Art. *IEEE Robot. Autom. Mag.*, vol. 23, no. 3, pp. 93–106, Sep. 2016.

[4] LAT Al Abeach, S Nefti-Meziani and S Davis. Design of a variable stiffness soft dexterous gripper. *Soft Robot.*, vol. 4, no. 3, pp. 274-284, Sept. 2017.

[5] JY Nagase, S Wakimoto, T Satoh, N Saga and K Suzumori. Design of a variable-stiffness robotic hand using pneumatic soft rubber actuators. *Smart Mater. Struct.*, vol. 20, no. 10, pp. 105015, Aug. 2011.

[6] A Stilli, HA Wurdemann and K Althoefer. Shrinkable, stiffness-controllable soft manipulator based on a bio-inspired antagonistic actuation principle. In *2014 IEEE/RSJ International Conference on Intelligent Robots and Systems (IROS)*, 2014, pp. 2476-2481.

[7] Y Wei, Y Chen, T Ren, Q Chen, C Yan, Y Yang and Y Li. A novel, variable stiffness robotic gripper based on integrated soft actuating and particle jamming. *Soft Robot.*, vol. 3, no. 3, pp. 134-143, Sept. 2016.

[8] Y Yang, Y Zhang, Z Kan, J Zeng and MY Wang. Hybrid Jamming for Bioinspired Soft Robotic Fingers. *Soft Robot.*, Nov. 2019.

[9] X Zeng, C Hurd, HJ Su, S Song and J Wang. A parallel-guided compliant mechanism with variable stiffness based on layer jamming. *Mech. Mach. Theory*, vol. 148, pp. 103791, Feb, 2020.

[10] Y Yang, Y Chen, Y Li, Z Wang and Y Li. Novel variable-stiffness robotic fingers with built-in position feedback. *Soft Robot.*, vol. 4, no. 4, pp. 338-352, Dec. 2017.

[11] W Wang, CY Yu, PAA Serrano and SH Ahn. Shape Memory Alloy-Based Soft Finger with Changeable Bending Length Using Targeted Variable Stiffness. Nov. 2019.

[12] J Santoso, EH Skorina, M Salerno, S de Rivaz, J Paik and CD Onal. Single chamber multiple degree-of-freedom soft pneumatic actuator enabled by adjustable stiffness layers. *Smart Mater. Struct.*, vol. 28, no. 3, pp. 035012, Feb. 2019.

[13] J Shintake, B Schubert, S Rosset, H Shea and D Floreano. Variable stiffness actuator for soft robotics using dielectric elastomer and low-melting-point alloy. In *2015 IEEE/RSJ International Conference on Intelligent Robots and Systems (IROS)*, 2015, pp. 1097-1102.

[14] C Chautems, A Tonazzini, D Floreano and BJ Nelson. A variable stiffness catheter controlled with an external magnetic field. In *2017 IEEE/RSJ International Conference on Intelligent Robots and Systems (IROS)*, 2017, pp. 181-186.

[15] TL Buckner, MC Yuen, SY Kim and R Kramer-Bottiglio. Enhanced Variable Stiffness and Variable Stretchability Enabled by Phase-Changing Particulate Additives. *Adv. Funct. Mater.*, vol. 29, no. 50, pp. 1903368, Oct. 2019.

[16] U Culha, J Hughes, A Rosendo, F Giardina, and F. Iida. Design Principles for Soft-Rigid Hybrid Manipulators. Springer, Cham, 2017, pp. 87–94.

[17] L Paternò, G Tortora, and A Menciassi. Hybrid Soft–Rigid Actuators for Minimally Invasive Surgery. *Soft Robot.*, vol. 5, no. 6, pp. 783–799, Dec. 2018.

[18] Z Shahid, AL Glatman and SC Ryu. Design of a Soft Composite Finger with Adjustable Joint Stiffness. *Soft Robot.*, vol. 6, no. 6, pp. 722–732, Dec. 2019.

[19] M Haghshenas-Jaryani, W Carrigan, and M B J Wijesundara. Design and Development of a Novel Soft-and-Rigid Hybrid Actuator System for Robotic Applications. in *Volume 5A: 39th Mechanisms and Robotics Conference*, 2015, p. V05AT08A047.

[20] Y Chen, S Le, Q C Tan, O Lau, F Wan, and C Song. A reconfigurable hybrid actuator with rigid and soft components. In *2017 IEEE International Conference on Robotics and Automation (ICRA)*, 2017, pp. 58–63.

[21] S Manjia, R Xie, Y Zhang, X Kang, D Huang, Y Guan, and H Zhu. Pneumatic Soft Actuator with Anisotropic Soft and Rigid Restraints for Pure in-Plane Bending Motion. Applied Sciences 9, no. 15 (2019): 2999.

[22] P Panagiotis, Z Wang, JTB Overvelde, KC Galloway, R J Wood, K Bertoldi, and C J. Walsh. Modeling of soft fiber-reinforced bending actuators. IEEE Transactions on Robotics 31, no. 3 (2015): 778-789.

[23] F Connolly, P Polygerinos, C J Walsh, and K Bertoldi. Mechanical Programming of Soft Actuators by Varying Fiber Angle. *Soft Robot.*, vol. 2, no. 1, pp. 26–32, Mar. 2015.

[24] P Polygerinos, Z Wang, K C Galloway, R J Wood, and C J Walsh. Soft robotic glove for combined assistance and at-home rehabilitation. *Rob. Auton. Syst.*, vol. 73, pp. 135–143, Nov. 2015.

[25] M D Andrew, RK Katzschmann, and D Rus. Whole arm planning for a soft and highly compliant 2d robotic manipulator. In 2014 IEEE/RSJ International Conference on Intelligent Robots and Systems, pp. 554-560. IEEE, 2014.